Metallurgical and Materials Engineering *Research paper*
Association of Metallurgical Engineers of Serbia AMES *https://doi.org/10.30544/766*

THE EFFECT OF MICROWAVE ENERGY ON SINTERING OF AN AUSTENITIC STAINLESS STEEL REINFORCED WITH BORON CARBIDE

Ederson Bitencourt das Neves [1], Edilson Nunes Pollnow[2], Alice Gonçalves Osorio[3]*

[1] School of Mechanical Engineering, Federal University of Rio Grande, 96203-900, Brazil
[2] School of Engineering, Federal University of Grande Dourados, 79825-070, Brazil
[3] School of Materials Engineering, Federal University of Pelotas, 96010-610, Brazil

Received 28.11.2021

Accepted 05.08.2022

Abstract

Microwave heating has emerged as an alternative to traditional sintering methods because it consumes less energy and requires shorter processing times. The use of microwave energy in the processing of austenitic stainless steel AISI 316L reinforced with dispersed boron carbide particles was investigated in this study. Different processing parameters were used to investigate the effect of sintering time and temperature, as well as the weight percentage of the ceramic added to the steel matrix, on the final material properties. The compressibility curve, elastic relaxation, and geometric density of green compacts were used to investigate their physical properties. The Archimedes method was used to determine density, and the statistical treatment of analysis of variance was used to determine porosity. Images obtained using optical microscopy and scanning electron microscopy revealed the formation of a second phase in different volumes. The results showed that 1100°C and a 15-minute plateau were sufficient to sinter the material. AISI 316L samples containing 3wt% boron carbide demonstrated greater volumetric formation of secondary phases, resulting in a significant increase in the hardness of the austenitic composite developed.

Keywords: Microwave sintering; AISI 316L; B_4C; steel making.

[*] Corresponding author: Neves, E.B., *edersonbn@gmail.com*

Introduction

Microwave sintering of metallic materials differs from traditional methods in that it provides volumetric heating with shorter processing cycles [1], and the thermal profile of the microwave sintering (MWS) is influenced by the particle size of the powders [2]. As a result, powders must have adequate particle size and distribution, as they will directly affect the sintering mechanisms, which are responsible for compacted densification [3]. MWS heating is based on a material's ability to absorb electromagnetic energy and, as a result, heat up quickly due to the action of Silicon Carbide (SiC) susceptors present inside the oven cavity, making the MWS action more energy efficient by heating microwave hybrids (MHH). Microwave energy promotes volumetric heating from the inside to the outside of the compact in the MHH, and the susceptors promote radiation heating from the outside to the inside (as in conventional heating of electric resistance ovens) [1, 4]. Metallic materials' sintering mechanisms are complex because they have different properties that result in different reactions to MWS radiation energy; even for the same type of metallic material and heating conditions, different levels of performance will occur due to selective heating in different samples [5]. When compared to conventional sintering methods, the physical-mechanical properties and microstructure obtained are uniform and have a lower porosity, with a reduction in processing time and lower energy consumption [6, 7, 8].

AISI 316L austenitic stainless steels are gaining popularity in a variety of applications due to their excellent corrosion resistance, good surface finish, and forming capacity. Despite its potential, this alloy is limited in its application due to its low hardness, which affects its wear resistance. A possible solution to this limitation is to incorporate a harder material into the austenitic matrix, thereby altering its mechanical properties.

Boron carbide (B_4C) stands out among the ceramic materials used to reinforce different metal matrix bases for its high hardness [9, 10]. It is also used as super abrasives in polishing; as a grinding medium; for sharpening cutting tools, sandblasting guns, and as a material for armoring vehicles and making bulletproof vests [11]. The unique combination of properties of B_4C makes it a material of choice for a wide range of industrial applications [12], including applications requiring low friction and low wear [13].

Hence, alternative processing technique could be an effective solution to avoid final cost increase. In that context, the aim of this study was to identify the optimum time and temperature of MWS of AISI 316L stainless steel reinforced with different B_4C additives as well as analyze the microstructure and hardness of the final composite. The results presented aim to increase the understanding of the effects of microwave energy on the formation of the microstructure of metallic materials.

Experimental procedures

The characterization of the powders was performed by morphology analysis using the scanning electron microscope (SSX-550 Superscan), average particle size by laser granulometry (CILAS 1064 granulometer), chemical analysis using Dispersive Energy X-Ray Fluorescence Spectrometer (EDX 720/800 HS) and X-ray diffraction phase analysis (Shimadzu XRD- 6000). Powder characteristics of the austenitic stainless steel AISI 316L used is described in Table 1 and in Table 2.

Table 1. AISI 316L powder characteristics.

Element	C	Mn	P	Si	Ni	Cr	Mo	N	Fe
wt%	0.03	2.00	0.04	0.75	10.6	17.7	2.13	0.10	Bal.
Particle size	90% of particles ≤ 204.87 μm 50% of particles ≤ 99.21 μm 10% of particles ≤ 51.16 μm								

Table 2. B_4C powder characteristics.

Type	Description		Surface area (BET) m²/g			Density in green	
Grid HS	Powder for sintering		15-20			1,6-1,8 g/cm³	
Element	Impurity levels Al	N	O	Fe	Si	C	B
wt%	0.05	0.70	1.70	0.05	0.15	21.80	Bal.
Particle size	90% of particles ≤ 3.93 μm 50% of particles ≤ 1.61 μm 10% of particles ≤ 0.57μm						

Based on the percentage of B_4C, the compacted samples were divided into four groups containing six samples each group, totaling a population of 24 samples: Group A (pure AISI 316L); Group B (AISI 316L + 1wt% B_4C); Group C (AISI 316L + 2wt% B_4C) and Group D (AISI 316L + 3wt% B_4C). The nomenclature used to characterize the samples was first to indicate the group (A, B, C and D) followed by plateau time (15 or 60 min) and sintering temperature (1000, 1050 or 1100°C).

The formulation was performed on an analytical balance (FA2204C) with 220g capacity and accuracy of 0.0001g. A "Y" type mill was used to mix the powder at 30 RPM for 60 minutes for each of the formulations. Each sample presented a mass of 3 ± 0.02g that were inserted in the compacting matrix.

The theoretical density of the mixture between AISI 316L steel powder and boron carbide powder (Table 2) was obtained using the mixing rule Eq. (1). Where ρ_T is the total mix density, (m_A) the specific masses of the 316L powder, (m_B) the boron carbide powder, (ρ_{TA}) the density of the 316L powder, and (ρ_{TB}) the boron carbide powder.

$$\rho_T = \frac{m_A + m_B}{\frac{m_A}{\rho_{TA}} + \frac{m_B}{\rho_{TB}}} \qquad 1$$

The samples were compacted in a double-ended uniaxial 1045 cylindrical steel die with 10mm diameter. The pressure used in the compaction to obtain a maximum green powder density was 750 MPa, determined by the compressibility curve [14]. The dimensional variation was estimated by the elastic recovery after compaction from the width variation of the compacted, in relation to the width of the matrix cavity.

The elastic recovery (ER) with L = width of the compacted and D = size of the cavity of the matrix, was estimated by the relation:

$$ER\ (\%) = \left[\frac{(L-D)}{D}\right] * 100 \qquad 2$$

The green density (D_g) was obtained by the geometric method, using Eq. 3. The mass and volume values were collected after the extraction of the compacts from the matrix. An average of 5 measurements for each of the 24 samples were performed, and the densities for each of the groups (A, B, C and D) were calculated according to Eq. 3, where D_g is the green density of compacted m=mass, r=radius and h=height.

$$D_g = \frac{m}{\pi r^2 h} \qquad 3$$

The samples were sintered using a microwave oven INTI (FMIC 1600) with susceptors composed of plates of Silicon Carbide (SiC) installed throughout the cavity of the oven, in order to generate a hybrid heating system (MHH). The thermocouple used was type "S"; the microwave oven controls the temperature with a microprocessor system; The cavity temperature ranges from 100°C to 1600°C with radiation generated by the 1200 W magnetron.

Density is the ratio of mass to volume of the solid and has a direct influence on the mechanical properties of products obtained by sintering. To determine the apparent density of the sintered samples, the Archimedes principle was applied [15].

The statistical analysis of the data was done by calculating the correlation coefficient to verify the relationship between the percentage of boron carbide in the stainless steel matrix and its porosity. In order to perform the statistical analysis, the analysis of variance (ANOVA) with F test was used, and later the Tukey averages comparison test with 5% error probability was applied.

For the microscopic analysis, it was necessary to perform a metallographic preparation of the samples according to ASTM E3-11 [16]. This included the cutting, embedding, sanding, polishing and chemical etching of the samples, with a 3% Nital solution. Sanding and polishing were performed on the MiniMet® 250 Semi-Automatic Polishing Machine with 80, 180, 320, 400, 600, 1200 and 2000 mesh grit sanders and for the 0.1μm grit alumina suspension polishing step. The microstructural and mechanical characterization of the sintered samples were performed by optical microscopy (OM), scanning electron microscopy (SEM) and Vickers microhardness (HV) tests. The OM analyses were performed in a light microscope of reflected light with a system of analysis of images attached. The equipment used was an Olympus optical microscope (BX41M-LED) with system of acquisition of digital images. SEM mappings were performed with the JEOL-SEM (JSM 6610L) equipped with JEOL JSM 6610LV ES, BSE, EDS NORAN System Detectors. The Vickers HV microhardness was performed with a Shimadzu automatic micro-durometer (HMV-2T) adopting as base the standard 24, with tests conducted using a load of (0.3 kgf) with load time of 10s [17]. Ten indentations were made on each sample (5 in the region of the matrix and 5 in the region of the secondary phase). The experimental procedure parameters are described in Figure 1, where each cell represents a working parameter. Ex: Sample of group A sintered at the temperature of 1000 °C for 15 minutes is indicated by (A1000/15).

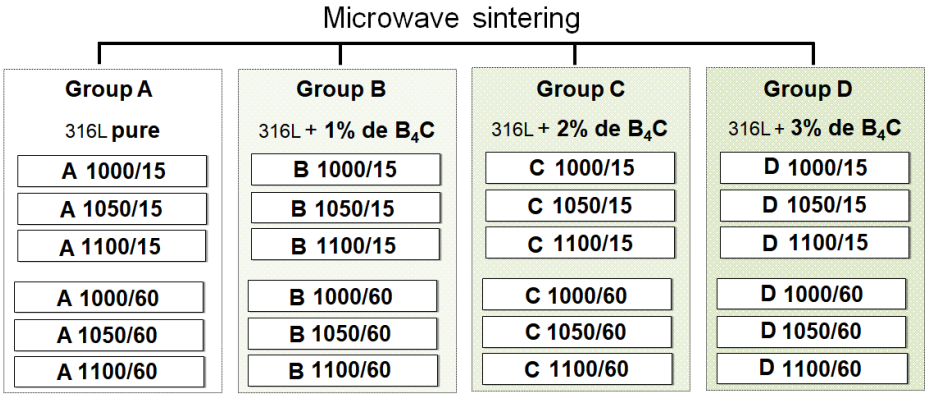

Fig. 1. Sintering parameters adopted in the present study.

Results and Discussion

The chemical composition analysis performed by EDX for pure AISI 316L powder presented 68.05 wt.% (Fe); 17.78 wt.% (Cr); 10.68 wt.% (Ni) and 2.13 wt.% (Mo). Fig. 2a and Fig. 2b show the morphology of the stainless steel and boron carbide powders.

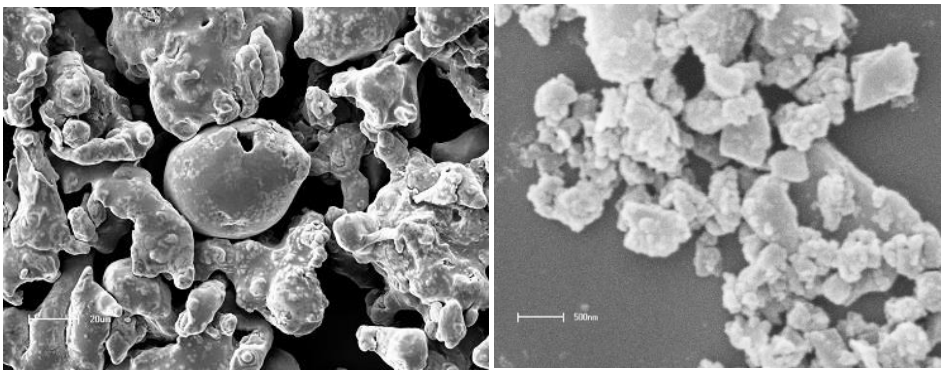

Fig. 2. Micrographs obtained by SEM: a) AISI 316L powder, b) boron carbide powder.

Both powders have an irregular and agglomerated morphology (Fig. 2a and Fig. 2b). The particle size test revealed that the stainless steel powder had an average particle size of 117.37 μm and the boron carbide had a particle size of 2.03 μm. The diameter of B4C powder is approximately 60 times smaller than that of 316L powder, which contributed to carbide dispersion during the mixing process with the austenitic alloy powder.

Figure 3 showed the XRD pattern obtained for SS316L with diffraction patterns 2θ peaks at (°) according to the JCPDS (033-0397).

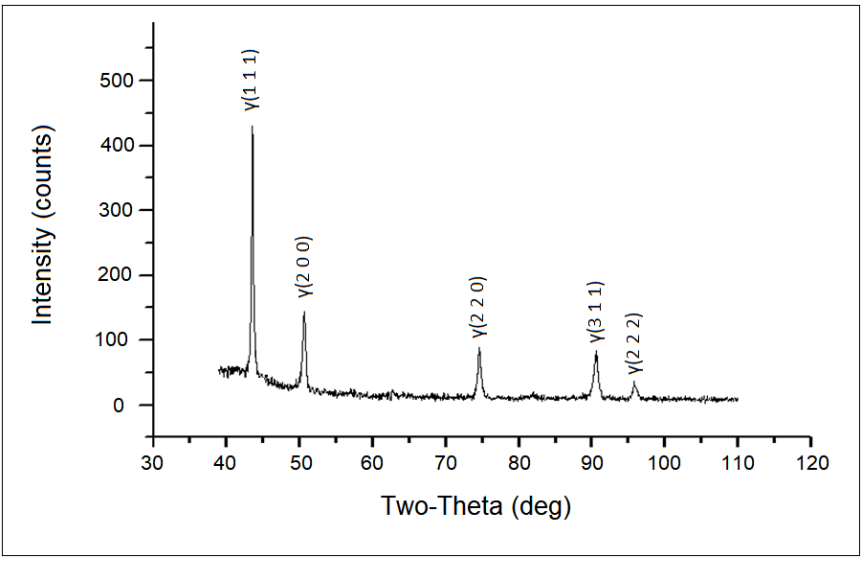

Fig. 3. XRD patterns from powder AISI 316L.

Figure 4 shows the XRD pattern obtained for B_4C with 2θ (°) diffraction peaks of boron carbide powder according to JCPDS crystallographic sheet (00-035-0798). There was also the presence of oxidized boron (B_3O_3) according to JCPDS (00-013-0570) and Aluminum Boron Carbide (Al0.84B39.82C4) described in the JCPDS sheet (01-077-0239).

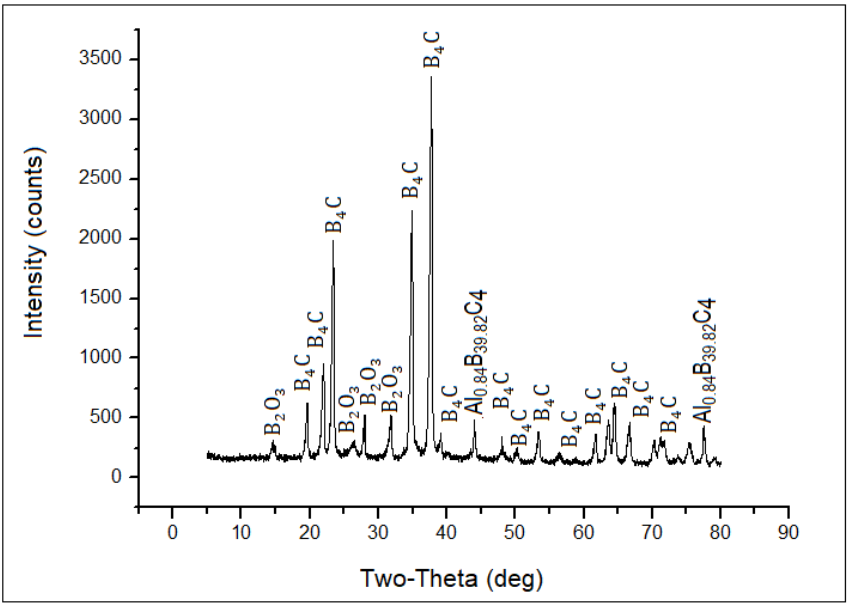

Fig. 4. XRD pattern from B_4C powder.

The "density versus pressure" curve indicates the compressibility of metal powders, delimiting the final compaction pressure where the curve will be established forming a straight line, indicating the optimum compacting pressure [18]. Compressibility curves for AISI 316L stainless steel powders with 1%, 2%, and 3% B_4C additions are shown in Fig. 5.

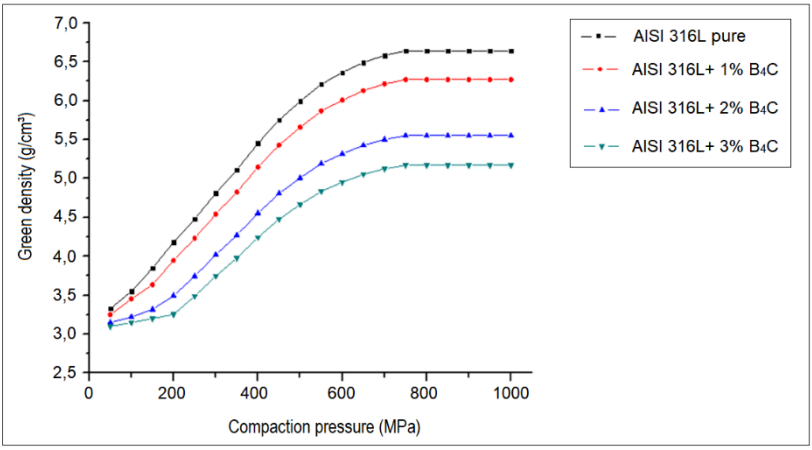

Fig. 5. Compressibility curves of 316L with B_4C powders.

The compressibility curves are shown in Fig. 5 as green density (g/cm3) of the compacted in relation to the applied pressure (MPa). The density decreased near 600 MPa, as indicated by a smaller slope of the curves, and became stable for pressures close to 750 MPa for all samples, where it remained constant up to 1GPa. Thus, based on the compressibility curve results, it is possible to confirm that all samples reached their optimum compaction pressure at 750 MPa. It has also been discovered that the addition of B_4C contributes to a reduction in green density.

It is possible to estimate how a series of components should be produced using powder metallurgy by analyzing the dimensional variation. Furthermore, it can indicate the effect of chemical composition on compressive pressure. The values of dimensional variation after matrix extraction are shown in Fig. 6.

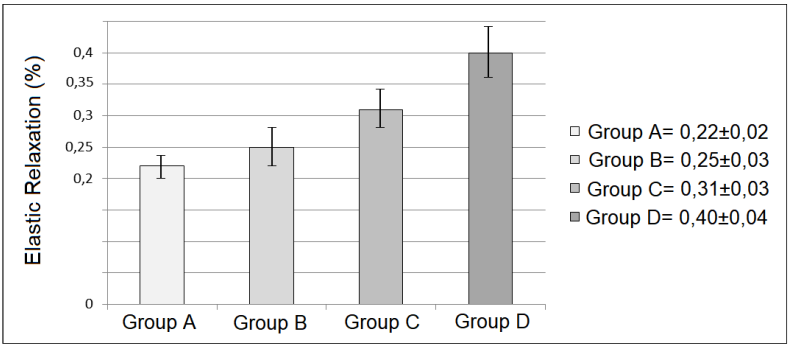

Fig. 6. Dimensional variation of Groups (A, B, C and D) represented by elastic relaxation after extraction of the matrix at a compaction pressure of 750 MPa.

The elastic relaxation after extraction is shown in Fig. 6 to be directly proportional to the addition of B_4C. When compared to pure stainless steel samples, the mixtures analyzed with 3% B_4C (Group D) show a greater volume increase (Group A). According to the authors, the higher elastic relaxation of samples with a higher B_4C percentage is due to the high hardness of these particles, which may not deform plastically during compaction, resulting in a larger elastic relaxation. Because it is based on the geometric method, the green density values confirm the elastic relaxation analysis. Table 3 depicts the apparent density values based on the theoretical densities obtained by (Equation 1).

Table 3. Green densification of the samples.

Groups of samples according to the percentage of B_4C	ρ theoretical (g/cm³)	ρ apparent* (g/cm³)	ρ relative (%)
Group A (AISI 316L pure)	8.05	6.64±0.003	83
Group B (AISI 316L+ 1% B_4C)	7.76	6.27±0.004	81
Group C (AISI 316L+ 2% B_4C)	7.49	5.54±0.005	74
Group D (AISI 316L+ 3% B_4C)	7.24	5.17±0.002	71

*calculated by the dimensions of the green compact.

According to the results, the pure stainless steel powder had a higher densification, which was reduced by the addition of the boron carbide powder. This reduction is thought to occur because B_4C particles are harder, making it difficult to pack the particles, that is, to approximate and plastically deform them, resulting in areas of less densification. Green density decreased by 3% for Group B and 14% for Group D as a result of a compacting pressure of 750 MPa. Following the collection of sample mass measurements (sintered compacts), equation 3 was applied, and the results of apparent density of each group, using the Archimedes a principle, are presented in Table 4.

Table 4. Density of sintered samples

Groups of samples according to the percentage of B_4C	ρ theoretical (g/cm³)	ρ real* (g/cm³)	ρ relative (%)
Group A (AISI 316L pure)	8.05	7.30±0.02	91
Group B (AISI 316L+ 1% B_4C)	7.76	6.65±0.05	86
Group C (AISI 316L+ 2% B_4C)	7.49	6.27±0.03	85
Group D (AISI 316L+ 3% B_4C)	7.24	6.08±0.04	84

*calculated by Archimedes principle.

Analyzing the apparent density (real) values, it is confirmed that the sintered density of the samples increased in comparison to the density of the green compacts due to the decrease of the pores, and this, in turn, remains smaller in comparison to theoretical density. When comparing the different plateau times used, there is still a small increase in sintering density as the plateau time increases, from 15 minutes to 60 minutes. It was also observed that there was a reduction in porosity with increasing plateau time, which may indicate that there was nothing is a coalescence of open pores with closed pores, in which there is a growth of the larger pores rather than the small ones.

The inclusion of boron carbide in the metal alloy caused differences in each group of samples. Groups B (AISI 316L + 1% B_4C) and C (AISI 316L + 2% B_4C) maintained constant density as temperature and sintering time increased. However, due to the addition of boron carbide to the metal alloy, "Group C" had a lower density than "Group B" and a higher density than "Group D." Finally, as the sintering time increased from 15 to 60 minutes, the density of "Group D" decreased.

The addition of B_4C to AISI 316L steel resulted in a decrease in the densification of the sintered samples, which was possibly increased by the percentage of pores present in the material. The increase in plateau time from 15 to 60 minutes to reduce the percentage of porosity appears to work only for pure stainless steel formulations with 1% and 2% B_4C. The influence is not supported by either plateau time or temperature. When 3% B_4C is added, the effect produced by the plateau time of 60 minutes reverses, resulting in an increase in the degree of porosity. The effect of sintering time and temperature on porosity can be seen in Table 5.

Because of the reduction in driving force, increasing the sintering plateau time for a given temperature is not always effective in decreasing porosity in MWS. The increase in porosity caused by a certain level of sintering can be attributed to a decrease in the absorption of the microwave radiation responsible for densification, resulting in the compacted material being influenced only by the thermal effect of the susceptor.

It is important to emphasize that analyzing the cause of variation in porosity using only the unit values of the samples is insufficient to predict the increase or decrease of the same. To obtain a more reliable result, the data was statistically treated using analysis of variance (ANOVA) based on the F test. The application of single-factor ANOVA (p<0,05) with 3 degrees of freedom found F= 34,45 and $F_{critical}$= 3,09. Thus, with ($F>F_{critical}$) and p=4x10^{-8}, a statistical difference was found between the four groups. However, only with the application of this test, it was not possible to determine the group (s) that had the greatest influence on the degree of porosity. Thus, a multiple comparison was made between the groups applying the *Tukey* test. The Tukey test (5%) showed that samples with B_4C presented a greater tendency to increase porosity. This allows us to deduce the effect of the ceramic powder addition in the stainless steel matrix on the degree of porosity. As the percentage of B_4C in the stainless steel alloy increases, the porosity increases as the sintering parameters (plateau time and temperature used in this work) are fixed. This is consistent with the results of this experimental study.

Table 5. Percentage of porosity in the sintered samples.

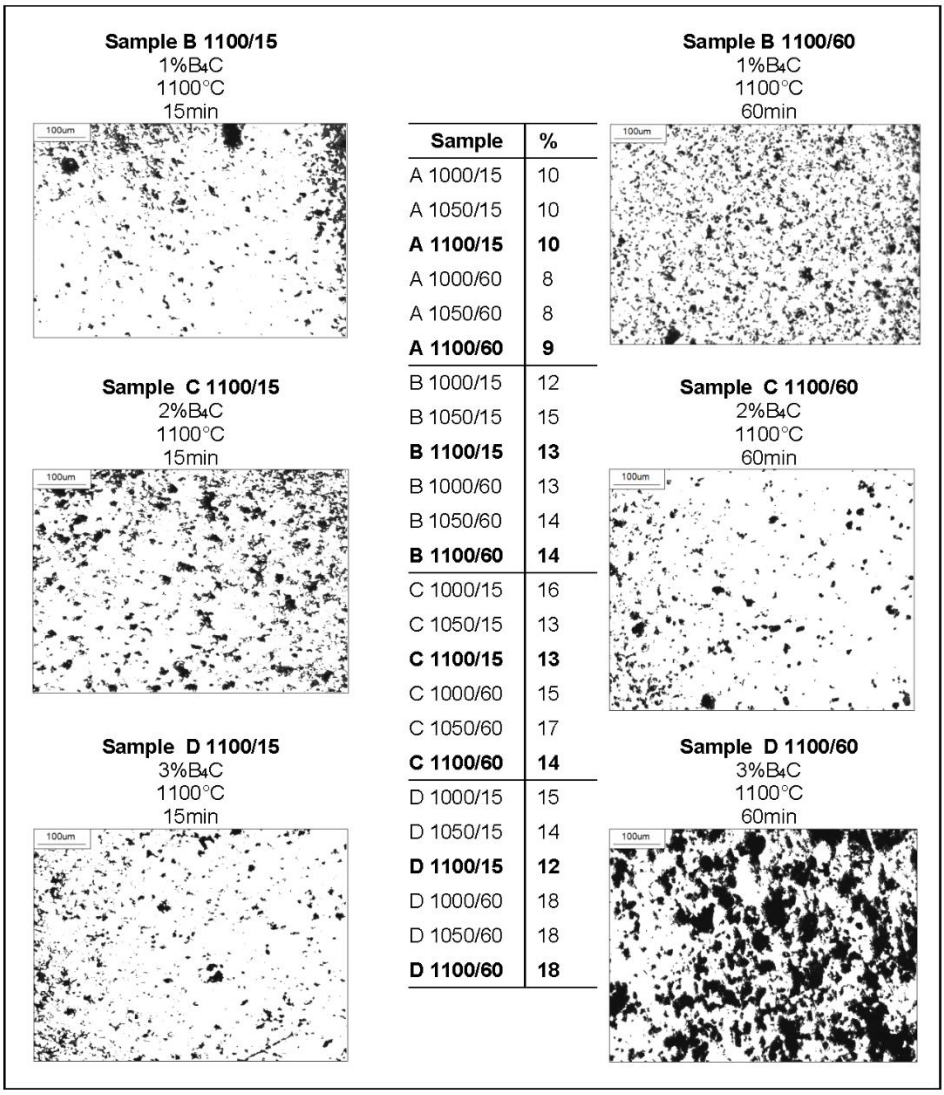

Sample	%
A 1000/15	10
A 1050/15	10
A 1100/15	**10**
A 1000/60	8
A 1050/60	8
A 1100/60	**9**
B 1000/15	12
B 1050/15	15
B 1100/15	**13**
B 1000/60	13
B 1050/60	14
B 1100/60	**14**
C 1000/15	16
C 1050/15	13
C 1100/15	**13**
C 1000/60	15
C 1050/60	17
C 1100/60	**14**
D 1000/15	15
D 1050/15	14
D 1100/15	**12**
D 1000/60	18
D 1050/60	18
D 1100/60	**18**

When microstructural analysis was performed, a second phase was seen. Hence, the microstructural characterization was performed in samples (A 1100/15), (B 1100/15), (C 1100/15) and (D 1100/15) representing the group of samples whose evolution of secondary phase formation is more apparent within each group (Fig. 7).

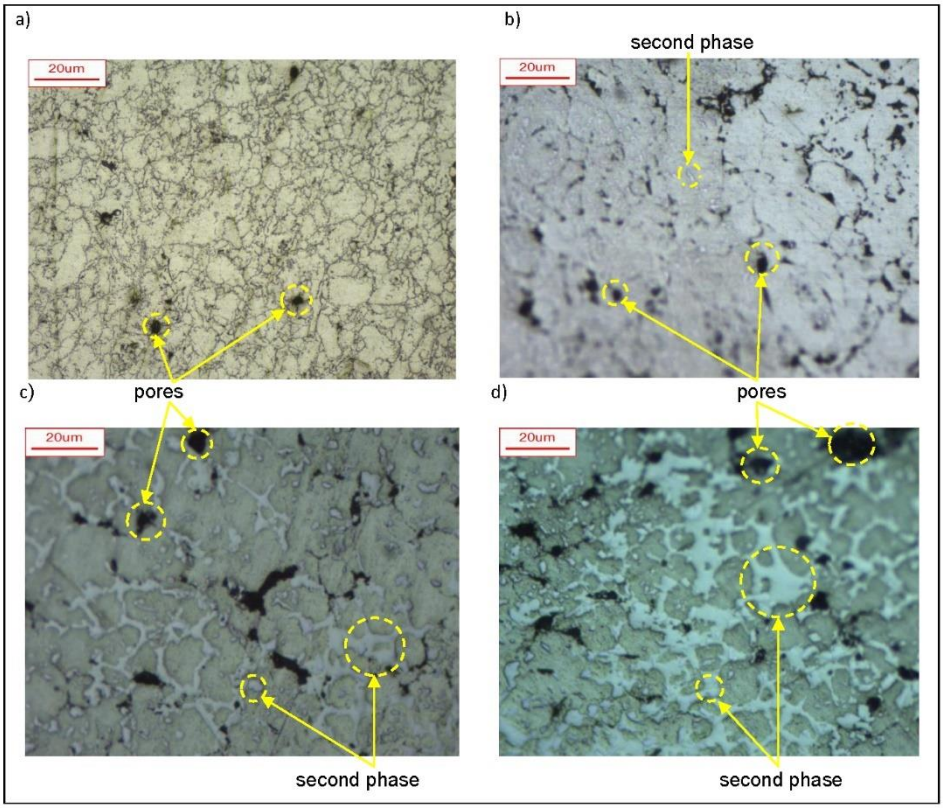

Fig. 7. OM images of the samples a) A 1100/15, b) B 1100/15, c) C 1100/15 e d) D 1100/15.

All pure stainless steel samples tested revealed only the austenitic matrix (Fig. 7a). MWS samples at lower temperatures and times showed good densification. When compared to conventional PM heating, which uses temperatures ranging from 1200 to 1400° [19, 20, 21], these results show that a shorter sintering temperature and plateau time can be used via MWS technique to obtain a PM 316L final product. Furthermore, *Panda et al.* [20] investigated the use of MWS in AISI 316L and obtained a 90% reduction in overall processing time through microwave sintering, but no improvement in densification or mechanical properties was observed. *Nagaraju* [21] examined MWS of 316L and concluded that densification increased, despite the fact that the working temperature was similar to that used in conventional sintering (1200 to 1300°C).

Fig.7b depicts the effects of adding 1wt% boron carbide to the AISI 316L steel matrix, which resulted in the formation of a small volume of second phase, possibly due to the presence of harder particles. Fig. 7c shows the sample C60/1100 (AISI 316L with 2wt% of B4C sintered at 1100°C for 60 min). When comparing this sample to the B15/1100 sample, it is possible to see a higher volumetric fraction of second phases. These findings imply that sintering time has a direct influence on the presence of a second phase.

Given that sample D15/1100 was sintered using the same sintering parameters as sample B15/1100, the fraction of second phase is accentuated (Fig. 7d). This result suggests that elastic relaxation may play an important role in the formation of a second phase. Based on the sintering results and micrographs, it can be assumed that the B_4C interacts with the 316L steel powder in some way, resulting in the formation of a second phase. Furthermore, the results show that sintering plateau time and elastic relaxation (related to sample density) play an important role in the formation of such second phase.

According to the authors, the second phase is caused by the high amount of carbon added in the form of a carbide, which dissociates and reacts with the elements of the matrix and the atmosphere when heated. When B_4C is added, the interaction with the environment may explain the increase in pores percentage. Figure 8 depicts the chemical analysis of a D15/1100 sample using the punctual EDS-BEC technique.

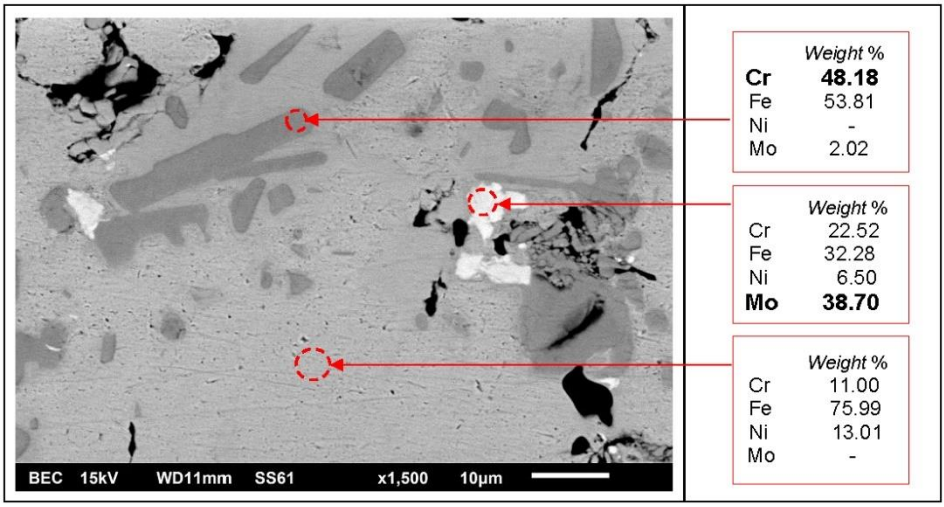

Fig. 8. Chemical analysis verified using punctual EDS-BEC technique in D15/1100 sample.

In Figure 8, it was possible to visualize the precipitation of two distinct phases, confirmed by chemical analysis of EDS, which indicated high chromium content in the darker tone phase and molybdenum precipitation in the lighter tone phase.

The austenitic matrix presented high percentage of nickel, as expected. For a better understanding of the phases present in the developed material, an in-line EDS technique was performed, which verified the chemical composition by a given path traced by a path represented by a line (vector). Fig. 9 shows the analysis performed by the in-line EDS technique in the D15/1100.

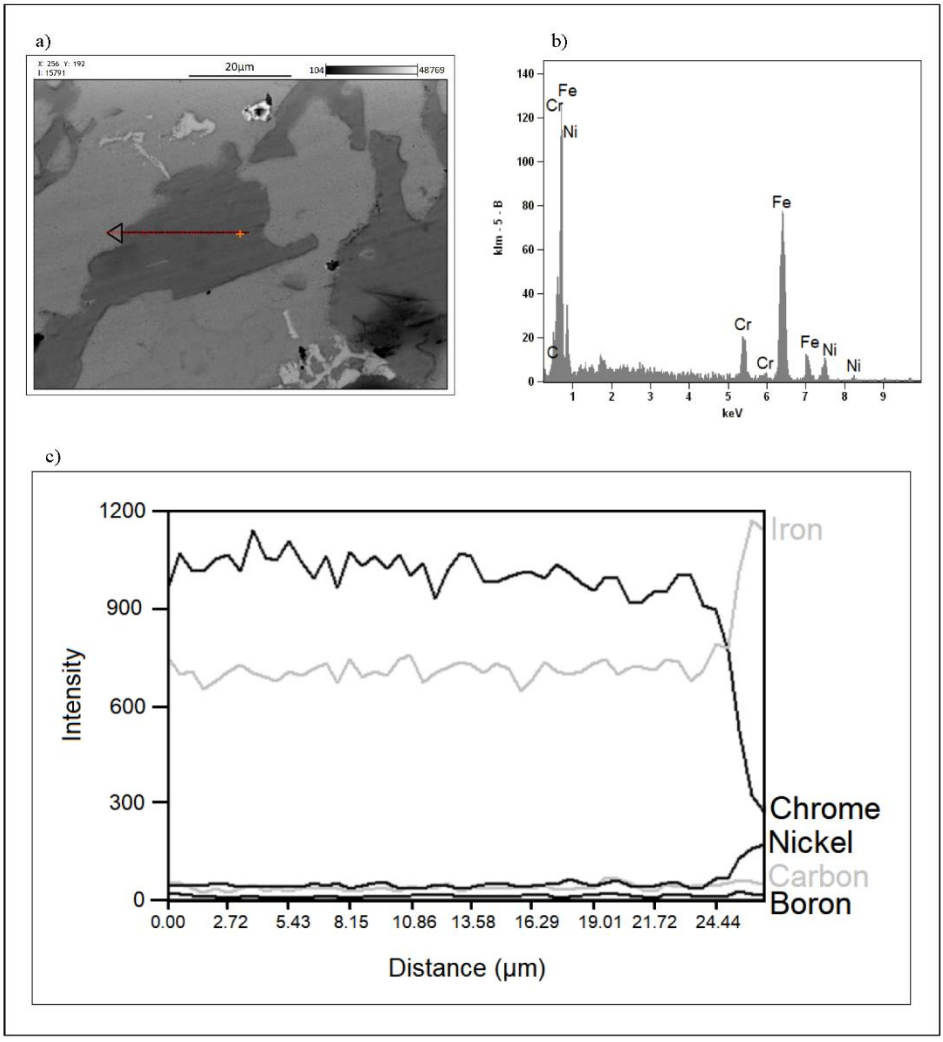

Fig. 9. Qualitative characterization of the elements present in the D15 / 1100 precipitate region by SEM. Image showing the vector used a), General spectrum obtained with in-line EDS-SEM b), graph representing the amount of elements along the vector c).

With the in-line EDS-SEM analysis of Sample D15 / 1100, it is confirmed that the dark tone second phase is rich in chromium with the matrix being formed by iron and nickel. This is evidenced by the inversion of intensity between the iron and chromium content after the distance of 24.44µm from the origin of the vector (EDS line – Figure 9c), where, when visualizing the micrograph (Figure 9a), it is verified that the end of the vector is located in the austenitic stainless steel matrix.

Vickers Microhardness (HV) characterization was, hence, performed in these different phases encountered in the microstructure. The analysis was based on the

division of two distinct areas, where the indentation was carried out: in the iron matrix and in the second phase, characterized by the difference of relief. In Table 6 the average values of microhardness per sample can be seen.

Table 6. Vickers microhardness values $HV_{0,3}$.

Group of samples as a function of the percentage of B_4C	Microhardness (Austenitic phase)	Microhardness (secondary phase)	Average Microhardness
Group A (AISI 316L pure)	97.73±5.50	-	97.73±5.50
Group B (AISI 316L+ 1% B_4C)	105±17.67	113.8±25.33	109±21.5
Group C (AISI 316L+ 2% B_4C)	116.2±16.5	154.57±42.5	135.38±29.5
Group D (AISI 316L+ 3% B_4C)	137.9±14.33	240.40±42.33	189.15±28.33

There was a relationship between parameter variation (addition of carbide, sintering plateau time and temperature) and hardness increase, with a gradual increase caused by the addition of boron carbide to the mixture. Fig. 10 shows the hardness of the 24 samples analyzed.

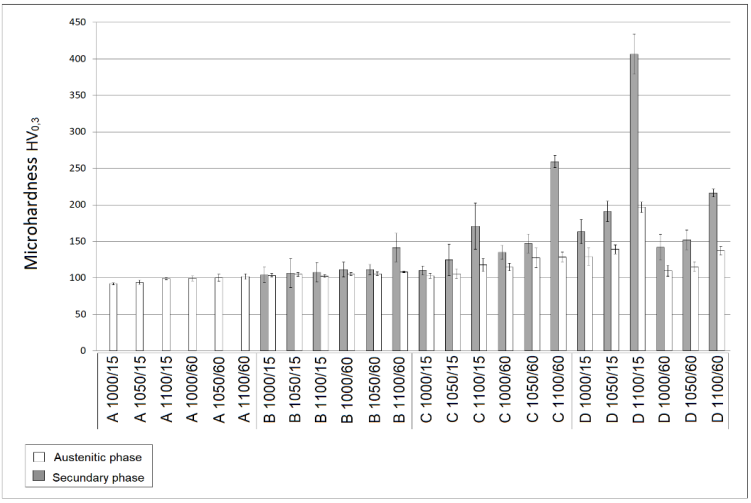

Fig. 10. Average microhardness values of all samples analyzed.

Based on the microhardness values in the austenitic matrix (Group A), a gradual increase in hardness was observed in groups B and C, with a highlight for sintered samples at temperatures of 1100 ° C and plateau times of 60 minutes. The addition of 3 wt.% ceramic powder, with sintering temperatures and times of 1100 °C and 15 min,

revealed the highest hardness value in both the steel matrix microhardness and the second phase. Values close to 406HV were obtained in the second phase, which is four times the value obtained in the sintered pure austenitic alloy under the same conditions. These values demonstrate that the second phases formed by the addition of boron carbide increase the material's hardness. However, when compared to the sample D15 / 1100, which remained in the oven for 14 of its time, these samples (3 wt.% B_4C sintered at 1100 °C for 60 min) had high porosity, which compromised the hardness of the compacted.

Based on data obtained and literature review, the authors suggest that the material developed indicates a decrease in production costs for PM 316L components, with a possible increase in hardness when little amount of B_4C in added to the stainless steel matrix.

Conclusions

The main conclusions for the use of MWS in the processing of the AISI 316L steel reinforced with dispersed boron carbide particles are as follows:

1. MWS induced volumetric heating in the samples, which affected the recrystallization kinetics and densified the austenitic matrix at lower rates of time and temperature, compared to conventional heating techniques commonly found in the literature.
2. The morphology present in samples with the addition of B_4C indicate the presence of distinct secondary phases, a phase rich in Cr (dark phase) and another phase in a lower amount rich in Mo (light phase). Both phases contribute to increase the hardness in the austenitic matrix.
3. For additions of 1% and 2% of B_4C by weight with 60 minutes of plateau, there was a small improvement in the reinforcement of the austenitic matrix.
4. Sample MWS sintered at 1100 °C for 15 minutes and 3% B_4C showed a high hardness, compared to the other samples. This result contributed to studies by MWS, since the optimization of the process was achieved in a shorter heating cycle.
5. MWS technique decreases the production costs for PM 316L components, with a possible increase in hardness when little amount of B_4C in added to the stainless steel matrix.

Acknowledgments

This work was supported by the Coordination for the Improvement of Higher Education Personnel (CAPES). In addition, the authors would like to thank the CEME-SUL/FURG for the characterization performed in the Center.

References

[1] D. Agrawal: Microwave sintering of the metal powders, In: I. Chang, Y. Zhao (Eds.), Advances in Powder Metallurgy, Woodhead Publishing, Cambridge, (2013) 361-379.

[2] R. R. Mishra, S. Rajesha, A. K. Sharma: Int J Adv Mech Eng, 4 (2014) 315-322.

[3] A. A. S. Inverno, “Efeito da radiação micro-ondas na sinterização em fases sólida e líquida de pós de aço inoxidável 316L”. https://repositorio.lneg.pt/handle/10400.9/3012 Accessed 15 March 2016.
[4] M. Bhattacharya, T. Basak: Energy, 97 (2016) 306-338.
[5] J. Sun, W. Wang, Q. Yue: Materials, 9 (2016) 231.
[6] S. Singh, D. Gupta, V. Jain: J Eng Manuf, 230 (2016) 603-6017.
[7] S. Bansal, D. Gupta, V. Jain: J Mater: Des Appl, 234 (2020) 881-894.
[8] R. Kumar, H. Bhowmick, D. Gupta, & S. Bansal: Proceedings of the Institution of Mechanical Engineers, Part L: Journal of Materials: Design and Applications, 235 (2021) 2310-2323.
[9] F. Thévenot: Journal of the European Ceramic Society, 6 (1990) 205-225.
[10] J. K. Sonber, T. S. R. Ch. Murthy, C. Subramanian, R. K. Fotedar, R. C. Hubli, A. K. Suri: Trans. Indian Ceram. Soc, 72 (2013) 100-107.
[11] A. K. Suri, C. Subramanian, J. K. Sonber, T. S. R.Ch. Murthy: International Materials Review, 55(2010) 4-40.
[12] V. Domnich, S. Reynaud, R.A. Haber, M. Chhowalla: J Am Ceram Soc, 94 (2011) 3605-3628.
[13] W. Zhang: Progress in Materials Science, 116 (2021) 100718.
[14] ASTM B331-95: Standard Test Method for Compressibility of Metal Powders in Uniaxial Compaction, (2002) ASTM International.
[15] ASTM C373-88: Standard Test Method for Water Absorption, Bulk Density, Apparent Porosity, and Apparent Specific Gravity of Fired Whiteware Products, (2006) ASTM International.
[16] ASTM E3-11: Standard Guide for Preparation of Metallographic Specimens, (2011) ASTM International.
[17] ASTM E384-11$^{\varepsilon 1}$: Standard Test Method for Knoop and Vickers Hardness of Materials, (2011) ASTM International.
[18] T. H. Schneider, L. V. Biehl, E. B. das Neves, J. L. B. Medeiros, J. A. de Souza, F. A. D. do Amaral: MethodsX, 6 (2019) 1919-1924.
[19] C.H. Ji, N.H. Loh, K.A. Khor, S.B. Tor: Mater Sci Eng, 1-2 (2001) 74-82.
[20] S.S. Panda, V. Singh, A. Upadhyaya, D. Agrawal: Scripta Materialia, 54 (2006) 2179-2183.
[21] K.V.V. Nagaraju, S. Kumaran, T. Srinivasa Rao: Materials Today: Proceedings, 27 (2020) 2066-2071.